Supporting information for: Mapping Charge Percolation in Flowable Electrodes Used in Capacitive Deionization

Marm B. Dixit,[†] Daniel Moreno,[‡] Xianghui Xiao,[¶] Marta C. Hatzell,[*,‡] and Kelsey B. Hatzell[*,†]

[1]

†*Department of Mechanical Engineering, Vanderbilt University, Nashville, Tn, 37203, USA*

‡*George W. Woodruff School of Mechanical Engineering, Georgia Institute of Technology, Atlanta, Ga, 30313, USA*

¶*National Synchrotron Light Source II, Brookhaven National Laboratory, Upton, NY, USA*

E-mail: *marta.hatzell@me.gatech.edu; *kelsey.b.hatzell@vanderbilt.edu

Phone: +1 404-385-4503

Materials and Methods

Tomography Studies, Reconstruction, and Data Analysis

Gridrec algorithm[S1] was used for tomographic reconstructions and Wavelet-Fourier ring filter removal[S2] and Paganin phase retrieval[S3] methods were applied. Subsequent image processing was carried out using Image J[S4] and MATLAB. Binarization of the reconstruction images were carried out using thresholding routines available within ImageJ. Pore size distribution[S5] plugin was used to estimate the porosity of the samples. The pore size distribution is given by the histogram of the sphere radii. Skeletonize 3D option of the BoneJ plugin[S6] was used to obtain a skeleton map of the solid phase in the sample. The output skeletonized stack was analyzed to estimate the geodesic and the Euclidean length of each branch. The Euclidean length is defined as the straight-line distance between two points in space and represents the shortest distance between the two points in Euclidean space.[S7] The geometric tortuosity of a given branch is calculated using the following formula:[S8]

$$\tau = \frac{l_{geodesic}}{l_{Euclid}} \tag{1}$$

A histogram of geometric tortuosity for the entire skeleton map is obtained and the mean value is reported as the geometric tortuosity.

Tortuosity values are estimated using Taufactor,[S9] an open-source simulation software. The software estimates ion flux across the solution space in the flow electrodes. Additionally it estimates tortuosity factors based on the flux through the input binarized volume, J_p and an equivalent completely dense control volume, J_{cv}. Binarized image stacks are used as input for the simulations. Steady state simulations are carried out on the binarized volumes to estimate the diffusive flux through the system. Two opposite faces in the desired direction are set at concentrations of 1 and 0 respectively, while the rest of the faces of the binarized volume have a zero flux boundary condition. The simulations are carried out until the flux converges

to a steady state value. Similar procedure is repeated in the other two direction. The diffusive flux through the sample is estimated using the equation (Eq. 2). Additionally, the software estimates the diffusive flux through an identical, completely dense control volume using similar boundary conditions (Eq. 3). Tortuosity factors along each direction are estimated using the ratio of the diffusive flux computed across the binarized volume and the completely dense control volume. The transport properties, size and concentration gradients are kept constant across both these volumes.

$$J_p = -A_{cv} D \frac{\epsilon}{\tau} \frac{C}{L_{cv}} \tag{2}$$

$$J_{cv} = -A_{cv} D \frac{C}{L_{cv}} \tag{3}$$

Simulations are carried out on at least three domains for 10 and 20 wt% suspensions along the three principle axes. The simulations are carried out on representative domain sizes obtained after optimization. Cummulative flux projections are shown along the three principle axes.

Flow-electrode Capacitive Deionization

The FCDI system (Figure 1) is comprised of a Model 857 Redox Flow Cell Test System (Scribner Associates, Inc., Southern Pines, North Carolina). The two containers for the flow electrode contain stir plates which enable continuous mixing of the electrode during testing. The flow cell (area Acell = 25 cm^2) consists of a polycarbonate flow channel (clear polycarbonate, 0.47 cm thickness) and gold-plated copper current collectors. Viton fluoroelastomer gaskets are applied on either side of both membranes to ensure proper sealing of the cell. The carbon slurries flow through two graphite plates with channels (1 mm width $\times$ 5 cm length $\times$ 1 mm depth, 33 channels total in a triple serpentine flow pattern) and the feed flows vertically through the center of the cell. The feed and electrode flow rates used during the experiment were 5 mL/min and 10 mL/min. The flow electrode (100 mL) consisted of a constant 100 mM concentration (Sigma-Aldrich, St. Louis, Missouri, ACS reagent, $\geq$99%),

with varying degrees of activated carbon (AC): at 5%, 10%, and 15% weight. The cell was charged and discharged for 1.5 hours at a voltage of 1.2 V to avoid water splitting. The feed conductivity was measured using an Orion Fisher Scientific 013005MD Versa Star Pro Benchtop conductivity meter, and the current through the cell was collected from the Flow Cell software. The charging-discharging process was run over 3 cycles. While this number of cycles was not enough to achieve ideal statistical results, the different cycles ensured that cell stability could be retained during cyclic operation in batch mode.

The purpose of these experiments was to confirm known trends in increasing salt removal with increasing AC concentrations. Evaluating the average salt adsorption rate (ASAR) is also a useful tool for quantifying the effectiveness of increasing salt removal at higher weight percentages. While salt removal may be higher with more AC used, the increased AC mass may reduce the overall ASAR. Additionally, if additional AC enhances ion transport through electromigration, this will require additional energy input to the cell during charging. Pumping energy can also increase due to the greater viscosity of larger carbon loads, but this was not directly quantified in this study.

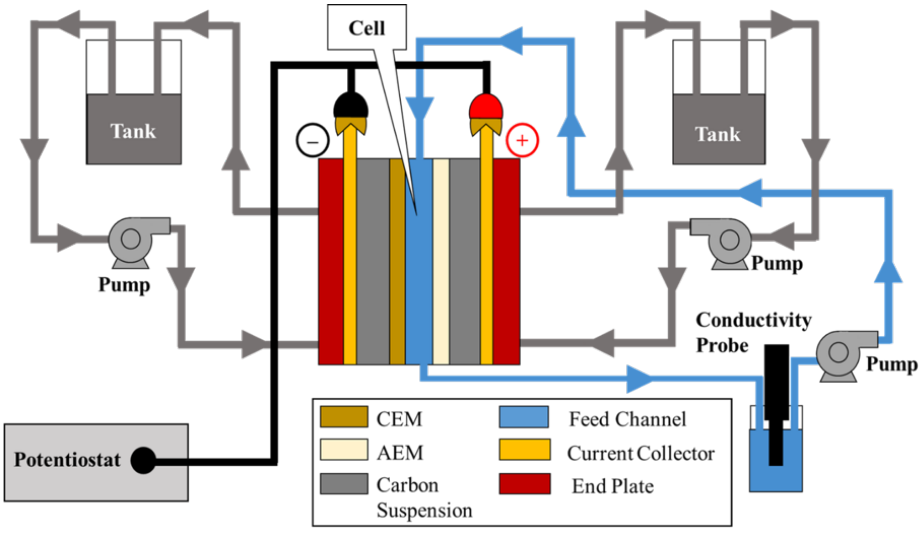

Figure S1: Batch mode flow electrode capactive deionization set-up.

References

(S1) Rivers, M. L. tomoRecon: High-speed tomography reconstruction on workstations using multi-threading. Developments in X-Ray Tomography VIII. 2012; p 85060U.

(S2) Münch, B.; Trtik, P.; Marone, F.; Stampanoni, M. Stripe and ring artifact removal with combined wavelet-Fourier filtering. *Optics Express* **2009**, *17*, 8567–8591.

(S3) Paganin, D.; Mayo, S. C.; Gureyev, T. E.; Miller, P. R.; Wilkins, S. W. Simultaneous phase and amplitude extraction from a single defocused image of a homogeneous object. *Journal of Microscopy* **2002**, *206*, 33–40.

(S4) Schneider, C. A.; Rasband, W. S.; Eliceiri, K. W. NIH Image to ImageJ : 25 years of Image Analysis. *Nature Methods* **2012**, *9*, 671–675.

(S5) Munch, B.; Holzer, L. Contradicting Geometrical Concepts in Pore Size Analysis Attained with Electron Microscopy and Mercury Intrusion. *Journal of Americal Ceramics Society* **2008**, *91*, 4059–4067.

(S6) Doube, M.; Klosowski, M. M.; Arganda-Carreras, I.; Cordelières, F. P.; Dougherty, R. P.; Jackson, J. S.; Schmid, B.; Hutchinson, J. R.; Shefelbine, S. J. BoneJ: Free and extensible bone image analysis in ImageJ. *Bone* **2010**, *47*, 1076–1079.

(S7) Jørgensen, P. S.; Hansen, K. V.; Larsen, R.; Bowen, J. R. Geometrical characterization of interconnected phase networks in three dimensions. *Journal of Microscopy* **2011**, *244*, 45–58.

(S8) Hormann, K.; Baranau, V.; Hlushkou, D.; Höltzel, A.; Tallarek, U. Topological analysis of non-granular, disordered porous media: determination of pore connectivity, pore coordination, and geometric tortuosity in physically reconstructed silica monoliths. *New J. Chem.* **2016**, *40*, 4187–4199.

(S9) Cooper, S. J.; Bertei, A.; Shearing, P. R.; Kilner, J. A.; Brandon, N. P. TauFactor: An open-source application for calculating tortuosity factors from tomographic data. *SoftwareX* **2016**, *5*, 203–210.